THE JOURNAL OF PHYSICAL CHEMISTRY LETTERS
A JOURNAL OF THE AMERICAN CHEMICAL SOCIETY

pubs.acs.org/JPCL

Letter

Construction and Structural Transformation of Metal–Organic Nanostructures Induced by Alkali Metals and Alkali Metal Salts

Rujia Hou,[†] Yuan Guo,[†] Zewei Yi, Zhaoyu Zhang, Chi Zhang,* and Wei Xu*

Cite This: *J. Phys. Chem. Lett.* 2023, 14, 3636–3642

Read Online

ACCESS | Metrics & More | Article Recommendations | Supporting Information

ABSTRACT: Metal–organic nanostructures are attractive in a variety of scientific fields, such as biomedicine, energy harvesting, and catalysis. Alkali-based metal–organic nanostructures have been extensively fabricated on surfaces based on pure alkali metals and alkali metal salts. However, their differences in the construction of alkali-based metal–organic nanostructures have been less discussed, and the influence on structural diversity remains elusive. In this work, from the interplay of scanning tunneling microscopy imaging and density functional theory calculations, we constructed Na-based metal–organic nanostructures by applying Na and NaCl as sources of alkali metals and visualized the structural transformations in real space. Moreover, a reverse structural transformation was achieved by dosing iodine into the Na-based metal–organic nanostructures, revealing the connections and differences between NaCl and Na in the structural evolutions, which provided fundamental insights into the evolution of electrostatic ionic interactions and the precise fabrication of alkali-based metal–organic nanostructures.

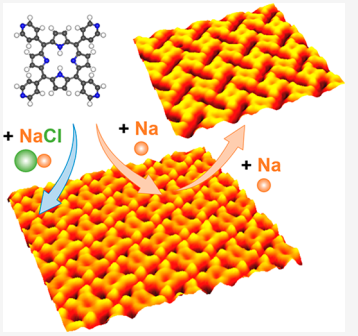

Metal–organic nanostructures, consisting of metal nodes and organic ligands, make up a class of structurally diverse and functionally tunable materials[1,2] and have proven to be versatile platforms in a wide range of scientific fields, including biomedicine, energy harvesting, and catalysis.[1,2] In an effort to achieve tailored properties and the desired performance, different types of metals have been integrated to regulate fundamental chemical interactions within building blocks, which range from transition metals to alkali and alkaline earth metals.[1−3] It has also aroused considerable interest in the surface science community; meanwhile, surface science techniques allow direct visualization of metal–organic nanostructures supported by solid surfaces in real space and determination of the intermolecular interactions involved. Tremendous effort has been devoted to the engineering of low-dimensional metal–organic architectures on surfaces mainly based on directional coordination bonds with d-block transition metals embedded,[4−6] as well as flexible coordination provided by f-block lanthanides.[7−9] Recently, alkali metals derived from either pure alkali metals[10−14] or alkali halides (e.g., NaCl and KBr)[15−22] have been introduced to interact with organic molecules on surfaces via isotropic electrostatic ionic bonding, enabling the structural diversity of metal–organic nanostructures.[10,14] In these cases, both pure alkali metals and alkali metal salts are applied to provide metal centers. However, their differences in the construction of alkali-based metal–organic nanostructures as alkali metal providers have been less discussed, and the corresponding influence on the structural diversity remains elusive. It is therefore of general interest to directly visualize and compare their roles in the construction of alkali-based metal–organic nanostructures as well as the induction of structural transformations, which would provide a fundamental understanding of alkali-based metal–organic interactions.

In this study, 5,10,15,20-tetra(4-pyridyl)-porphyrin [H_2TPyP (Scheme 1)] was selected as the target organic molecule, which is functionalized with four pyridyl groups serving as potential sites of interaction with Na.[15,19,22] The pure alkali metal Na and the typical alkali halide NaCl were applied as Na providers. By a combination of high-resolution scanning tunneling microscopy (STM) imaging and density functional theory (DFT) calculations, we have constructed Na-based metal–organic nanostructures and visualized the structural transformations in real space, which directly elucidates the role of Na and NaCl in the evolution of electrostatic ionic interactions. At a low Na/H_2TPyP stoichiometric ratio, the introduction of Na in the form of either NaCl or pure Na into the self-assembled H_2TPyP structures on Au(111) led to the construction of close-packed Na-based metal–organic nanostructures (Scheme 1). Further increasing the dosage of NaCl resulted in the coexistence of such close-packed nanostructures and additional NaCl islands, where the molecular arrangement remained undisturbed. Interestingly, after dosing of additional pure Na, in contrast,

Received: March 14, 2023
Accepted: April 6, 2023

https://doi.org/10.1021/acs.jpclett.3c00681
J. Phys. Chem. Lett. 2023, 14, 3636–3642

Scheme 1. Schematic Illustration Showing the Formation of Na-Based Metal−Organic Nanostructures Composed of H_2TPyP and Na and Their Structural Transformations on Au(111) in Response to NaCl and Na, Respectively[a]

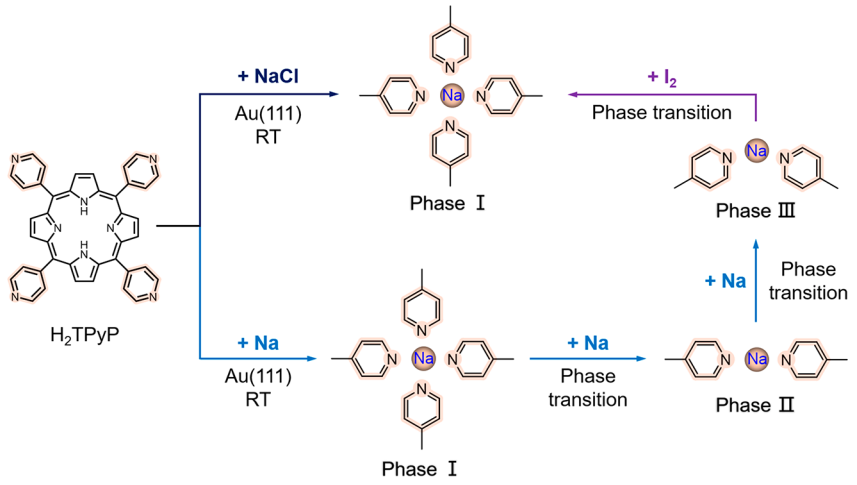

[a]The four pyridyl groups of the H_2TPyP molecule are highlighted to clearly show the intermolecular interactions with Na.

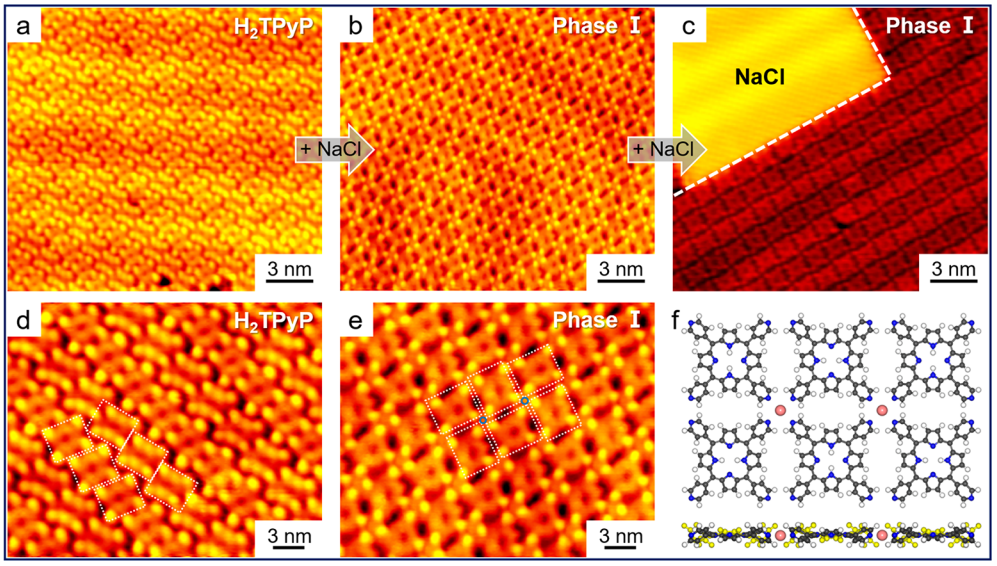

Figure 1. Structural transformation of H_2TPyP molecules on Au(111) in response to the dosage of NaCl. (a) Large-scale and (d) close-up STM images showing the self-assembled H_2TPyP islands on Au(111) upon deposition at ∼300 K. (b) Large-scale and (e) close-up STM images showing the formation of close-packed metal−organic nanostructures (phase I) after deposition of NaCl onto the H_2TPyP-precovered sample held at ∼300 K. The individual H_2TPyP molecules and Na atoms are depicted as dotted rectangles and filled circles, respectively. (c) Large-scale STM image showing the coexistence of phase I and additional NaCl islands after a NaCl overdose at ∼300 K, as separated by white dashed lines. Scanning conditions: V_t = −1.2 V, and I_t = 0.6 nA. (f) Top and side views of the DFT-optimized structural model showing the molecular arrangement of phase I. The molecules on the back from the side view are highlighted for the sake of clarity: gray for C, white for H, blue for N, and pink for Na.

a stepwise structural transformation in response to the Na dosage was observed, with the eventual formation of well-ordered Na-based metal−organic frameworks. Furthermore, DFT calculations revealed that the electrostatic ionic interactions between pyridyl groups and Na played a significant role in the stabilization of Na-based nanostructures involved in the evolution processes, and the structural transformation was driven by the increase in thermodynamic stability that originated from additional Na. In addition, by dosing iodine into the Na-based metal−organic frameworks, we achieved the reverse structural transformation back to the close-packed nanostructures (Scheme 1), indicating the competition between halogens (either Cl or I) and organic molecules in interacting with Na. These findings demonstrate a feasible strategy for constructing various alkali-based metal−organic nanostructures and clarifying the connections and differences between NaCl and Na in the structural evolutions, which would shed light on the precise fabrication and functionalization of alkali-based metal−organic nanostructures.

Deposition of H_2TPyP molecules onto Au(111) held at ∼300 K resulted in the formation of well-ordered self-assembled structures (Figure 1a). A high-resolution STM image showed that H_2TPyP molecules with the same adsorption direction were aligned in a row, and every two adjacent molecular rows were densely packed together, extending to form the molecular islands (Figure 1d) as reported previously.[22−24] Individual H_2TPyP molecules could be identified as depicted by white rectangles, appearing in 2-

https://doi.org/10.1021/acs.jpclett.3c00681
J. Phys. Chem. Lett. 2023, 14, 3636−3642

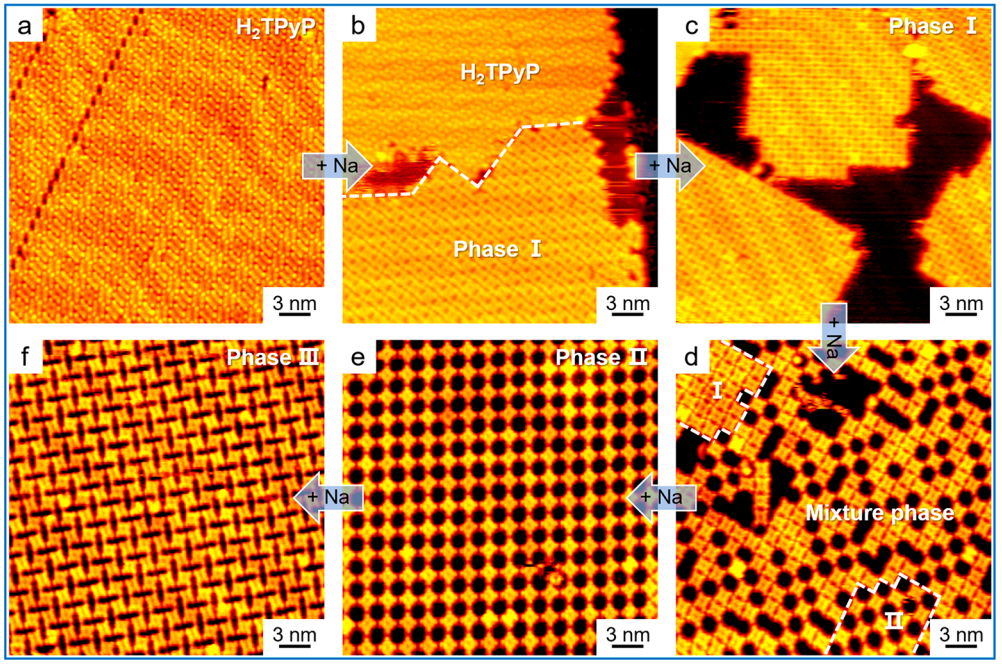

Figure 2. Structural transformation of H_2TPyP molecules in response to the dosage of Na on Au(111). (a–f) STM images showing the stepwise structural transformation from (a) self-assembled H_2TPyP structures, through (b) coexistence of self-assembled H_2TPyP and phase I, (c) phase I, (d) a mixture phase with the coexistence of phases I and II, (e) phase II, and eventually (f) phase III, along with the addition of Na to the sample held at ∼300 K. The borders of two coexisting phases are indicated by white dashed lines. Scanning conditions: V_t = −1.2 V, and I_t = 0.5 nA.

fold symmetric saddle-shaped morphologies, and four tilted pyridyl groups were shown as bright protrusions at the four edges, in line with previous reports.[22−24] To explore the interaction between alkali metal Na and H_2TPyP molecules, NaCl was first applied as the source of Na[16,17,19,21] and sublimated onto the H_2TPyP-precovered Au(111) substrate held at ∼300 K. After deposition of NaCl, a distinct molecular structure (defined as phase I) appeared (Figure 1b), in which every four neighboring H_2TPyP molecules were gathered in a square pattern and two adjacent molecules were perpendicular to each other (Figure 1e). In addition, four pyridyl rings from neighboring molecules formed a "four-leaf clover". A dark protrusion could be visible at the center in a special tip state (as depicted by blue circles in Figure 1e) and was attributed to Na according to our previous reports,[18,25] which is also in good agreement with the situation on Ag(111).[22] Furthermore, additional NaCl was deposited to verify the influence of NaCl dosage on the structural diversity, which, interestingly, led to the coexistence of NaCl islands and phase I (Figure 1c), while no structural transformation was observed. DFT calculations were further carried out on the structure of phase I, and the energetically most favorable one is shown in Figure 1f. From the top and side views, it can be seen that every four pyridyl groups interact with one Na via electrostatic interactions between N and Na,[15,19,22] and pyridyl groups are highly tilted due to the intra- and intermolecular steric hindrance. Note that the remaining Cl decomposed from NaCl could not be easily trapped or imaged under our experimental conditions in the absence of specific intermolecular interactions[26] between Cl and molecules, which has often been the case in previous reports.[17,21] In addition, changing the deposition sequence produced the same metal−organic nanostructure (i.e., phase I), and NaCl acts as a Na-supplying agent.

Next, to compare the role of pure Na in the structural transformation, Na was dosed in a stepwise manner into the H_2TPyP-precovered Au(111) sample (Figure 2a) held at ∼300 K. Initially, at a low Na/H_2TPyP stoichiometric ratio (<1), partial H_2TPyP consumed all Na forming phase I (same as the structure obtained in the case of NaCl), which led to the coexistence of phase I and the remaining H_2TPyP islands (Figure 2b). With an increasing Na dosage, H_2TPyP islands completely disappeared and transformed into phase I (Figure 2c), which also experimentally verified that the construction of phase I was related to only Na but independent of Cl. Interestingly, by continuously dosing Na into the former sample, we found rectangular cavities gradually appeared in the close-packed phase I (Figure S1) and a porous mixture phase thus formed (Figure 2d). In this porous phase, a majority of the H_2TPyP molecules interact with each other by gathering two pyridyl groups in a face-to-face mode, leaving two rectangular vacancies nearby, and some by gathering three pyridyl groups, leaving an adjacent vacancy. It was thus proposed that the additional Na would tend to form further ionic interactions with N from pyridyl groups and consequently disrupt the close-packed phase I. After the dosing of more Na, a well-ordered porous metal−organic nanostructure (phase II) was obtained, with every two pyridyl groups facing each other (Figure 2e). On the basis of such a structure, unexpectedly, the deposition of extra Na induced a further phase transition to another porous structure with smaller elliptical cavities [phase III (Figure 2f)]. Within phase III, H_2TPyP molecules rotated a bit and were no longer perpendicular or parallel to the adjacent ones, like that displayed in the molecular arrangement of phase II. It is noteworthy that phase III was available at only a high molecular coverage, while no phase transition (from II to III) was observed at a low coverage. To further verify the effect of Na on the phase transition, a series of reverse experiments were conducted on the basis of the sample covered with phase III, and additional H_2TPyP molecules were deposited step by step

https://doi.org/10.1021/acs.jpclett.3c00681
J. Phys. Chem. Lett. 2023, 14, 3636−3642

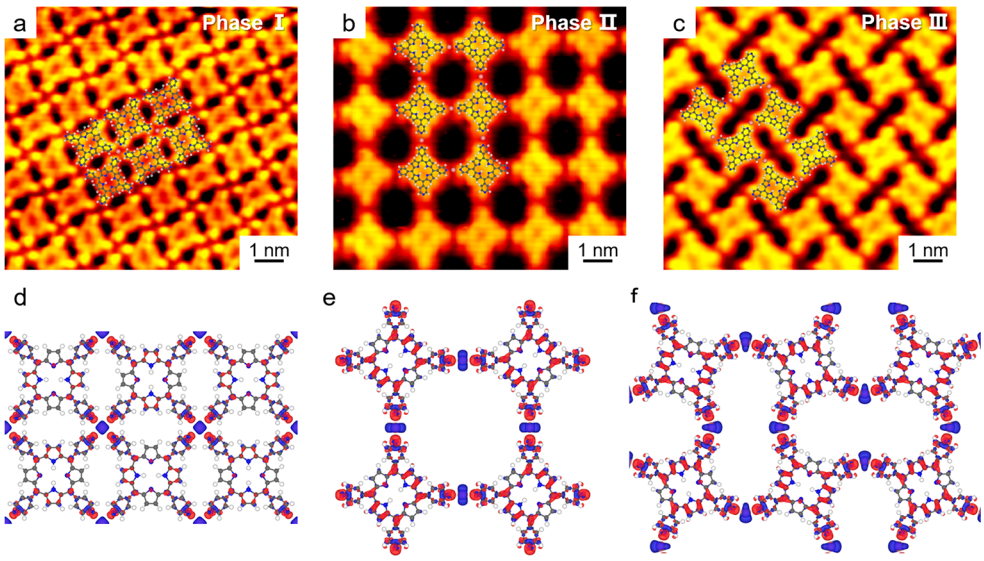

Figure 3. STM topographies of three kinds of metal−organic nanostructures and the corresponding charge-density-difference maps. (a−c) Close-up high-resolution STM images of phases I−III, respectively, superimposed with the corresponding DFT-optimized models. Scanning conditions: V_t = −1.2 V, and I_t = 0.5 nA. (d−f) Charge-density-difference maps of the corresponding structures showing the electrostatic ionic bonding between Na and N from pyridyl groups at an isosurface value of 0.002 e Å^{-3}. The red and blue isosurfaces indicate charge accumulation and depletion, respectively: gray for C, white for H, blue for N, and pink for Na.

Table 1. Electrostatic Potential Maps of Three Metal−Organic Phases and the Corresponding Binding Energies Involved[a]

	Phase I	Intermediate phase	Phase II	Phase III
Electrostatic potential map	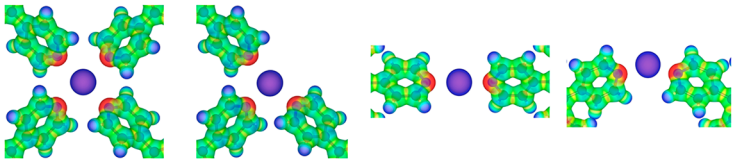			
Stoichiometric ratio [Na:H_2TPyP]	1:1	4:3	2:1	2:1
Binding energy [eV/H_2TPyP]	-3.64	-3.93	-4.02	-4.18
Binding energy [eV/Na]	-3.64	-2.95	-2.01	-2.09

[a]Red and blue colors represent negative and positive potential regions, respectively.

at a sample temperature of ∼300 K. As expected, with a decrease in the Na/H_2TPyP stoichiometric ratio, the transformation from phase III to I could be achieved, as well (Figure S2), which was responsive to both components involved.

To determine the metal−organic structures involved, extensive DFT calculations were carried out on the basis of the closed-up STM topographies of three different phases as typically shown in Figure 3a−c. With the addition of Na, the number of clustered pyridyl groups decreased, ranging from 4 (phase I) to 3 and 2 (mixture phase) to 2 (phase III). Note that in the mixture phase, several interaction modes coexist, and cavities are randomly distributed. As the phase transition depends on the Na dosage and no specific intermolecular interactions can be formed among pyridyl groups, the pyridyl groups should be gathered by forming, breaking, and re-forming electrostatic interactions with Na during the evolution process. Accordingly, the corresponding structures were theoretically calculated, and the DFT-optimized structural models were superimposed on the STM images (Figure 3a−c) with good agreement. Notably, an individual Na node can be surrounded by four, three, or two pyridyl rings via electrostatic interactions, which gives rise to the multiple metal−organic nanostructures. The comparison between phases II and III shows the flexibility of electrostatic interactions,[10] with each molecule rotated by a small angle. In addition, in the case of phase III, two identical metal−organic nanostructures could be clearly identified with different cavity sizes (Figure S3), further suggesting the flexible electrostatic interactions between Na and N. Moreover, charge-density-difference maps (Figure 3d−f) verified the electrostatic ionic bonding between Na and adjoining N atoms from pyridyl rings, where obvious charge

https://doi.org/10.1021/acs.jpclett.3c00681
J. Phys. Chem. Lett. 2023, 14, 3636−3642

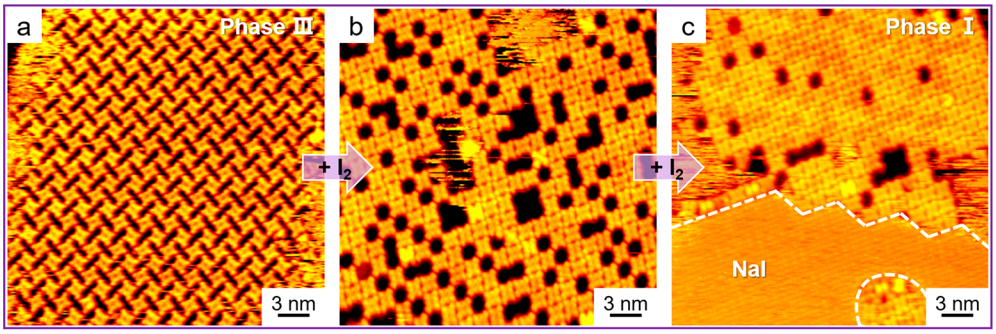

Figure 4. Structural transformation of porous metal−organic nanostructures in response to the dosage of iodine on Au(111). STM images showing the reverse structural transformation from (a) phase III, through (b) a mixture phase, and eventually to (c) the coexistence of phase I and NaI islands by gradually exposing the sample to an iodine atmosphere held at ∼300 K. The border of NaI islands is indicated by white dashed lines. Scanning conditions: V_t = −1.2 V, and I_t = 0.5 nA.

transfer could be observed. In addition, close inspection of the STM images of phase III revealed the presence of excess Na in the elliptical cavities (Figure S4), which rationalized the destination of additional Na atoms compared to the situation in phase II. As a result, depending on the Na dosage, a series of structural evolutions were obtained, which is distinct from the assembly process using NaCl, even though both are known as Na suppliers.

Furthermore, the interesting question of what causes the difference between NaCl and Na in inducing the phase transition arises. To reveal the driving force of such an evolution, we quantified the electrostatic ionic interactions involved in these structures by calculating the corresponding binding energies (Figure S5). The electrostatic potential maps along with the binding energies were calculated on the basis of the optimized periodic structural models (Figure 3) and are shown in Table 1. From the electrostatic potential maps, it can be recognized that all nitrogen atoms from pyridyl rings are negatively charged, while the Na atoms are positively charged in all of these structures, which also qualitatively elaborates the electrostatic interactions as the dominant ones. During the addition of Na, the binding energy per H_2TPyP molecule increases progressively with the Na/H_2TPyP stoichiometric ratio, from −3.64 to −3.93 to −4.02 to −4.18 eV/molecule. This means that when more Na atoms are embedded in the molecular system, the excess Na tends to disrupt the former electrostatic interactions to form thermodynamically more favorable structures with the certain number of coexisting H_2TPyP molecules instead of existing separately, which causes the structural evolution from phase I to phase III. In contrast, when excess NaCl is supplied, the extra NaCl forms well-ordered NaCl islands with considerable ionic interactions between Na and Cl, rather than providing Na for further integration into the molecular structures. Considering the binding energy per Na, conversely, the phase transition is a thermodynamically unfavorable process for NaCl, as the binding energy within these structures decreases (from −3.64 to −2.95 to −2.01 to −2.09 eV/Na) during this process. Thus, after the construction of phase I via consumption of all of the coexisting H_2TPyP molecules, Na derived from NaCl prefers to stabilize Cl as NaCl islands, instead of participating more thoroughly in the metal−organic structures while leaving the decomposed Cl alone. The competition from the ionic bonding between Na and Cl plays a crucial role in the progress of structural transformations, which determines the distinct evolution scenarios in the cases of Na and NaCl. Moreover, such evolution processes are thermodynamically driven, which is dependent on the differences in the stabilities of the corresponding structures.

Thereafter, STM experiments were conducted to experimentally understand the correlations between the cases of NaCl and Na and induce the interconversions. The porous phase III obtained on the basis of H_2TPyP and Na at a stoichiometric ratio of ∼2/1 (as described in Figure 2) was selected as the starting phase (Figure 4a) and was then exposed to an iodine atmosphere in a stepwise manner (Figure 4). The sample was first exposed to iodine at a pressure of ∼1 × 10^{-8} mbar for 10 min, resulting in the structural transformation to a less ordered mixture phase (Figure 4b) with clustering of H_2TPyP molecules, which is similar to the case in Figure 2d and indicates a decreasing Na/H_2TPyP stoichiometric ratio in the range of 1/1 to 2/1 in the corresponding nanostructures. Moreover, after dosing of additional iodine at a pressure of ∼5 × 10^{-8} mbar for 10 min, a nearly close-packed metal−organic nanostructure (phase I) was constructed with the formation of NaI islands, and some molecules were found to be embedded in the NaI islands (Figure 4c). This control experiment further validates the role of halogen atoms in the structural evolution, which grab additional Na from the metal−organic nanostructures, leading to the reverse phase transition. Such a transformation corresponds well to the situation shown in Figure 1 and to the scenario from the theoretical results discussed above.

Notably, in the previous studies, NaCl is generally known as an insulating support for decoupling[27,28] and has been recently introduced to interact with various molecular systems in the following situations. (i) Only Na cations are directly involved in the metal−organic nanostructures, forming electrostatic ionic interactions,[15−22,29] similar to the cases of pure alkali metals. (ii) Na interacts with organic molecules to construct the metal−organic motifs, while halogens further stabilize the structures, leading to structural diversity.[26,30] (iii) NaCl tightly binds together and simultaneously interacts with organic molecules, forming NaCl−organic coordinated nanoarchitectures.[31,32] In contrast, in this study, the competition among several types of electrostatic interactions is shown, which directly elucidates the role of halogen species (the counterpart of Na) in structural formation and transformation.

In conclusion, on the basis of STM imaging and DFT calculations, the alkali-based metal−organic nanostructures were constructed by using pure alkali metals and alkali metal

https://doi.org/10.1021/acs.jpclett.3c00681
J. Phys. Chem. Lett. 2023, 14, 3636−3642

salts, while structural transformations were induced by pure alkali metals. Both Na and NaCl can provide sodium to form electrostatic interactions with H_2TPyP molecules, and the presence of halogens was shown to prevent the structural transformation, which was experimentally elaborated by addition of iodine to the Na-based nanostructures. Furthermore, DFT calculations reveal that the increase in the thermodynamic stability accounts for such a structural transformation. Our results demonstrate the connections and differences between NaCl and Na in the structural evolutions at the molecular scale, which would pave the way for the precise fabrication of alkali-based metal−organic nanostructures.

■ ASSOCIATED CONTENT

Supporting Information

The Supporting Information is available free of charge at https://pubs.acs.org/doi/10.1021/acs.jpclett.3c00681.

Additional experimental methods, supplementary STM images of gradual structural evolution processes, identical metal−organic nanostructures with different cavity sizes, the presence of excess Na in the elliptical cavities in phase III, and DFT-optimized structural models used to calculate binding energies (PDF)

■ AUTHOR INFORMATION

Corresponding Authors

Wei Xu − *Interdisciplinary Materials Research Center, School of Materials Science and Engineering, Tongji University, Shanghai 201804, People's Republic of China;* orcid.org/0000-0003-0216-794X; Email: xuwei@tongji.edu.cn

Chi Zhang − *Interdisciplinary Materials Research Center, School of Materials Science and Engineering, Tongji University, Shanghai 201804, People's Republic of China;* orcid.org/0000-0002-2335-4579; Email: zhangchi11@tongji.edu.cn

Authors

Rujia Hou − *Interdisciplinary Materials Research Center, School of Materials Science and Engineering, Tongji University, Shanghai 201804, People's Republic of China*

Yuan Guo − *Interdisciplinary Materials Research Center, School of Materials Science and Engineering, Tongji University, Shanghai 201804, People's Republic of China*

Zewei Yi − *Interdisciplinary Materials Research Center, School of Materials Science and Engineering, Tongji University, Shanghai 201804, People's Republic of China*

Zhaoyu Zhang − *Interdisciplinary Materials Research Center, School of Materials Science and Engineering, Tongji University, Shanghai 201804, People's Republic of China*

Complete contact information is available at: https://pubs.acs.org/10.1021/acs.jpclett.3c00681

Author Contributions

†R.H. and Y.G. contributed equally to this work.

Notes

The authors declare no competing financial interest.

■ ACKNOWLEDGMENTS

The authors acknowledge financial support from the National Natural Science Foundation of China (Grants 22125203, 21790351, and 22202153), the Fundamental Research Funds for the Central Universities, and Covestro. The authors are grateful for the use of RIKEN's HOKUSAI supercomputer system.

■ REFERENCES

(1) Ye, G.; Chen, C.; Lin, J.; Peng, X.; Kumar, A.; Liu, D.; Liu, J. Alkali /Alkaline Earth-Based Metal−Organic Frameworks for Biomedical Applications. *Dalton Trans* **2021**, *50*, 17438−17454.

(2) Jiao, L.; Seow, J. Y. R.; Skinner, W. S.; Wang, Z. U.; Jiang, H.-L. Metal−Organic Frameworks: Structures and Functional Applications. *Mater. Today* **2019**, *27*, 43−68.

(3) Matlinska, M. A.; Ha, M.; Hughton, B.; Oliynyk, A. O.; Iyer, A. K.; Bernard, G. M.; Lambkin, G.; Lawrence, M. C.; Katz, M. J.; Mar, A.; et al. Alkaline Earth Metal−Organic Frameworks with Tailorable Ion Release: A Path for Supporting Biomineralization. *ACS Appl. Mater. Interfaces* **2019**, *11*, 32739−32745.

(4) Stepanow, S.; Lin, N.; Barth, J. V. Modular Assembly of Low-Dimensional Coordination Architectures on Metal Surfaces. *J. Phys.: Condens. Matter* **2008**, *20*, 184002.

(5) Dong, L.; Gao, Z. A.; Lin, N. Self-Assembly of Metal−Organic Coordination Structures on Surfaces. *Prog. Surf. Sci.* **2016**, *91*, 101−135.

(6) Zhang, Y.; Zhang, X.; Li, Y.; Zhao, S.; Hou, S.; Wu, K.; Wang, Y. Packing Sierpiński Triangles into Two-Dimensional Crystals. *J. Am. Chem. Soc.* **2020**, *142*, 17928−17932.

(7) Écija, D.; Urgel, J. I.; Papageorgiou, A. C.; Joshi, S.; Auwärter, W.; Seitsonen, A. P.; Klyatskaya, S.; Ruben, M.; Fischer, S.; Vijayaraghavan, S.; et al. Five-Vertex Archimedean Surface Tessellation by Lanthanide-Directed Molecular Self-Assembly. *Proc. Natl. Acad. Sci. U. S. A.* **2013**, *110*, 6678−6681.

(8) Urgel, J. I.; Écija, D.; Auwärter, W.; Stassen, D.; Bonifazi, D.; Barth, J. V. Orthogonal Insertion of Lanthanide and Transition-Metal Atoms in Metal−Organic Networks on Surfaces. *Angew. Chem., Int. Ed.* **2015**, *54*, 6163−6167.

(9) Moreno, D.; Parreiras, S. O.; Urgel, J. I.; Muñiz-Cano, B.; Martín-Fuentes, C.; Lauwaet, K.; Valvidares, M.; Valbuena, M. A.; Gallego, J. M.; Martínez, J. I.; et al. Engineering Periodic Dinuclear Lanthanide-Directed Networks Featuring Tunable Energy Level Alignment and Magnetic Anisotropy by Metal Exchange. *Small* **2022**, *18*, 2107073.

(10) Shan, H.; Zhou, L.; Ji, W.; Zhao, A. Flexible Alkali−Halogen Bonding in Two Dimensional Alkali-Metal Organic Frameworks. *J. Phys. Chem. Lett.* **2021**, *12*, 10808−10814.

(11) Ding, Y.; Xie, L.; Li, D.; Shen, H.; Li, C.; Xu, W. Interconversion between Guanine Quartets and Triads on the Au(111) Surface. *Chem. Commun.* **2022**, *58*, 3198−3201.

(12) Stepanow, S.; Ohmann, R.; Leroy, F.; Lin, N.; Strunskus, T.; Wöll, C.; Kern, K. Rational Design of Two-Dimensional Nanoscale Networks by Electrostatic Interactions at Surfaces. *ACS Nano* **2010**, *4*, 1813−1820.

(13) Li, D.; Ding, Y.; Wang, X.; Xu, W. On-Surface Fabrication of Bimetallic Metal−Organic Frameworks through the Synergy and Competition among Noncovalent Interactions. *J. Phys. Chem. Lett.* **2021**, *12*, 5228−5232.

(14) Wang, X.; Ding, Y.; Li, D.; Xie, L.; Xu, W. Linear Array of Cesium Atoms Assisted by Uracil Molecules on Au(111). *Chem. Commun.* **2019**, *55*, 12064−12067.

(15) Wäckerlin, C.; Iacovita, C.; Chylarecka, D.; Fesser, P.; Jung, T. A.; Ballav, N. Assembly of 2D Ionic Layers by Reaction of Alkali Halides with the Organic Electrophile 7,7,8,8-Tetracyano-P-Quinodimethane (TCNQ). *Chem. Commun.* **2011**, *47*, 9146−9148.

(16) Shimizu, T. K.; Jung, J.; Imada, H.; Kim, Y. Supramolecular Assembly through Interactions between Molecular Dipoles and Alkali Metal Ions. *Angew. Chem., Int. Ed.* **2014**, *53*, 13729−13733.

(17) Skomski, D.; Abb, S.; Tait, S. L. Robust Surface Nano-Architecture by Alkali-Carboxylate Ionic Bonding. *J. Am. Chem. Soc.* **2012**, *134*, 14165−14171.

(18) Zhang, C.; Wang, L.; Xie, L.; Kong, H.; Tan, Q.; Cai, L.; Sun, Q.; Xu, W. Solventless Formation of G-Quartet Complexes Based on Alkali and Alkaline Earth Salts on Au(111). *ChemPhysChem* **2015**, *16*, 2099−2105.
(19) Liu, X.; Matej, A.; Kratky, T.; Mendieta-Moreno, J. I.; Günther, S.; Mutombo, P.; Decurtins, S.; Aschauer, U.; Repp, J.; Jelinek, P.; et al. Exploiting Cooperative Catalysis for the On-Surface Synthesis of Linear Heteroaromatic Polymers via Selective C−H Activation. *Angew. Chem., Int. Ed.* **2022**, *61*, No. e202112798.
(20) Chen, C.; Ding, P. C.; Li, Z.; Shi, G. Q.; Sun, Y.; Kantorovich, L. N.; Besenbacher, F.; Yu, M. Super-Robust Xanthine−Sodium Complexes on Au(111). *Angew. Chem., Int. Ed.* **2022**, *61*, No. e202200064.
(21) Zhang, C.; Xie, L.; Wang, L.; Kong, H.; Tan, Q.; Xu, W. Atomic-Scale Insight into Tautomeric Recognition, Separation, and Interconversion of Guanine Molecular Networks on Au(111). *J. Am. Chem. Soc.* **2015**, *137*, 11795−11800.
(22) Zhou, K.; Liang, H.; Wang, M.; Xing, S.; Ding, H.; Song, Y.; Wang, Y.; Xu, Q.; He, J. H.; Zhu, J.; et al. Fine-Tuning of Two-Dimensional Metal−Organic Nanostructures via Alkali−Pyridyl Coordination. *Nanoscale Adv.* **2020**, *2*, 2170−2176.
(23) Auwärter, W.; Écija, D.; Klappenberger, F.; Barth, J. V. Porphyrins at Interfaces. *Nat. Chem.* **2015**, *7*, 105−120.
(24) Auwärter, W.; Weber-Bargioni, A.; Riemann, A.; Schiffrin, A.; Gröning, O.; Fasel, R.; Barth, J. V. Self-Assembly and Conformation of Tetrapyridyl-Porphyrin Molecules on Ag(111). *J. Chem. Phys.* **2006**, *124*, 194708.
(25) Ding, Y.; Wang, X.; Li, D.; Xu, W. Real-Space Evidence of Trimeric, Tetrameric, and Pentameric Uracil Clusters Induced by Alkali Metals. *J. Phys. Chem. C* **2020**, *124*, 5257−5262.
(26) Xie, L.; Ding, Y.; Wang, X.; Xu, W. Chlorine-Assisted Fabrication of Hybrid Supramolecular Structures via Electrostatic Interactions. *Phys. Chem. Chem. Phys.* **2019**, *21*, 9357−9361.
(27) Wang, Y.; Kröger, J.; Berndt, R.; Tang, H. Molecular Nanocrystals on Ultrathin Nacl Films on Au(111). *J. Am. Chem. Soc.* **2010**, *132*, 12546−12547.
(28) Pavliček, N.; Gross, L. Generation, Manipulation and Characterization of Molecules by Atomic Force Microscopy. *Nat. Rev. Chem.* **2017**, *1*, 0005.
(29) Skomski, D.; Tait, S. L. Ordered and Robust Ionic Surface Networks from Weakly Interacting Carboxyl Building Blocks. *J. Phys. Chem. C* **2013**, *117*, 2959−2965.
(30) Xie, L.; Zhang, C.; Ding, Y.; E, W.; Yuan, C.; Xu, W. Structural Diversity of Metal−Organic Self-Assembly Assisted by Chlorine. *Chem. Commun.* **2017**, *53*, 8767−8769.
(31) Hieulle, J.; Peyrot, D.; Jiang, Z.; Silly, F. Engineering Two-Dimensional Hybrid NaCl−Organic Coordinated Nanoarchitectures on Metal Surfaces. *Chem. Commun.* **2015**, *51*, 13162−13165.
(32) Guo, Q.; Huang, M.; Lu, S.; Cao, G. Ionic Compound Mediated Rearrangement of 3, 4, 9, 10-Perylene Tetracarboxylic Dianhydride Molecules on Ag(100) Surface. *Nanotechnology* **2015**, *26*, 275603.

https://doi.org/10.1021/acs.jpclett.3c00681
J. Phys. Chem. Lett. 2023, 14, 3636−3642